Yan et al. Journal of Palaeogeography (2019) 8:2
https://doi.org/10.1186/s42501-018-0017-z

Journal of Palaeogeography

RESEARCH Open Access

Using geophysical logs to identify Milankovitch cycles and to calculate net primary productivity (NPP) of the Late Permian coals, western Guizhou, China

Zhi-Ming Yan[1], Long-Yi Shao[1*], David Large[2], Hao Wang[1] and Baruch Spiro[3]

Abstract

Milankovitch periodicities of 123 kyr (eccentricity), 35.6 kyr (obliquity), and 21.2 kyr (precession) were identified in geophysical logs of three Late Permian coals: 17#, 18#, and 17 + 18#, from the Songhe mining area in western Guizhou Province. Based on the astronomic temporal framework, the periods of deposition of the 17# (5.6 m), 18# (6.4 m), and 17 + 18# (5.4 m) coals were constrained to 140.8–119.8 kyr, 160–136.2 kyr, and 135–114.9 kyr, respectively. The overall depositional period of the 18# coal of 160–136.2 kyr was further subdivided using the wavelet analysis method, into short and precise periods corresponding to the Milankovitch periodicities. It includes one eccentricity periodicity (123 kyr), three obliquity periodicities (35.6 kyr), and five precession periodicities (21.2 kyr). Different thicknesses of the subdivided coal sections, equivalent to the same time span of deposition, indicate different rates of coal deposition, i.e., thicker sections imply higher rates while the thinner sections represent lower rates. The combination of the measured average carbon concentration with the density of the coals gave rise to long-term average values of carbon accumulation rates for the Late Permian coals, in the range of 42.4–50.6 $g \cdot C \cdot m^{-2} \cdot a^{-1}$. This range corresponds to the long-term average carbon accumulation rates for the initial peat in the range of 60.6–72.3 $g \cdot C \cdot m^{-2} \cdot a^{-1}$. Based on the known quantitative relation between net primary productivity (NPP) values and long-term average carbon accumulation rates for the Holocene tropical peatlands, the range of NPP values for the Late Permian tropical peatlands was estimated as 242.4–433.8 $g \cdot C \cdot m^{-2} \cdot a^{-1}$.

A comparison of existing information about peatland NPP levels of various ages and latitudes indicated that when conditions of high rain and high humidity prevail in the palaeo-peatland at given latitude, the NPP rates will vary with changes in atmospheric concentration of CO_2 and O_2. This relationship may lead to the use of coals as an indicator for the concentration of these gases (CO_2 and O_2) in the contemporaneous atmosphere encompassing the long records of coal deposition.

Keywords: Milankovitch cycle, Coal deposition, Peatland, Long-term average carbon accumulation rate, Net primary productivity, Late Permian, Guizhou Province

* Correspondence: shaol@cumtb.edu.cn
[1]College of Geoscience and Surveying Engineering, China University of Mining and Technology (Beijing), Beijing 100083, China
Full list of author information is available at the end of the article

1 Introduction

Peatlands are globally important terrestrial carbon pools and vital components of soil-atmosphere carbon exchange processes (Vitt 1994; Page et al. 2011; Large and Marshall 2014). Recent research has suggested that approximately one-third of the global organic soil carbon is stored in peatlands (Mitsch and Gosselink 2007). The organic carbon productivity-decay balance plays a significant role in global carbon cycles, and is also critical to climatic variation (Yu et al. 2014). This indicates that the understanding of the long-term behavior of peatland carbon reservoirs is increasingly significant. Most peatland carbon is contained within subarctic, boreal, and postglacial peat deposits, which are mostly less than 10 kyr old. These features limit much of our understanding of the characteristics and evolution of high- to mid-latitude and pre-Quaternary peatlands (Kremenetski et al. 2003; Yu 2011). Much of the geological record of peat derived carbon is contained in thick pre-Quaternary coal deposits. Therefore, coal deposits can be used to investigate the evolution of older peatlands (Large and Marshall 2014).

To make use of pre-Quaternary coal deposits as a proxy for palaeoclimatic analysis, it is necessary to develop internal and absolute temporal frameworks based on whole coal seams. These provide the basis for estimating long-term average carbon accumulation rates, and the understanding of the synchronous evolution of peatland carbon reservoirs (Large and Marshall 2014). By utilizing the potential of coals containing evidence of orbitally paced environmental change, the temporal framework of the coal seam can be established. The key is the identification of Milankovitch cycles from indicative geochemical or geophysical data in coal (Weedon 2003) and then estimating reasonable upper and lower limits of the period of deposition for the coal via the corresponding lengths and periodicities of orbital cycle (Large and Marshall 2014). This process has already been successfully applied to the Cenozoic coal and lignite deposits (Briggs et al. 2007; Large 2007; Large and Marshall 2014). According to the combination of the measured average carbon concentration and the coal density, and the carbon loss during coalification, the likely range of the original long-term average carbon accumulation rate for the peatlands can be estimated (Large 2007). This result then can give rise to the calculation of peatland net primary productivity (NPP) based on the quantitative relation between the long-term average carbon accumulation rate for the peatland and the NPP level during a specific period.

These approaches are based on an assumption of a degree of uniformitarianism, and are largely dependent on information from the Holocene peatland as well. This is likely to be one of a few approaches applied to improve our understanding of the ecology of peatland formed during pre-Quaternary times.

In this study, spectral analysis was conducted on geophysical logs, such as apparent resistivity, gamma-gamma and natural-gamma logs of three relatively thick Late Permian coal seams in the Songhe mining area in western Guizhou. Results of the spectral analysis lead to the identification of the Milankovitch cycles. The temporal long-term average carbon accumulation rate for the peatland as well as regional peatland productivity were estimated based on a temporal framework constrained by these Milankovitch cycles. Furthermore, we subdivided the whole period of coal deposition into several short and precise periods for the construction of an internal temporal framework based on the wave curves corresponding to specific orbital frequencies. Finally, the main factors influencing the productivity of the peatland were assessed.

2 Geological settings

The Songhe mining area is situated in northern Panzhou City, western Guizhou Province (Fig. 1). It is a part of the Yunnan-Guizhou-Sichuan-Chongqing coal-rich zone in Southwest China. During the Late Permian, this coal-rich zone was one part of a stable intra-cratonic basin within the western Yangtze Block of the South China microcontinent. It was located between the Kangdian Oldland to the west and the Cathaysian Landmass to the east (Liu 1990; Liu et al. 1993; Wang and Jin 2000). The western Guizhou Province was located at a palaeolatitude of about 2.5°S (Wang and Li 1998) during the Late Permian. This region was dominated by warm and wet palaeoclimates that favored peat-forming plant communities (Han and Yang 1980; Liu 1990; Li and Wu 1996; Wang and Jin 2000).

The Upper Permian in the study area includes the basal Emeishan Basalt Formation consisting of massive basalts and the overlying coal-bearing siliciclastic Xuanwei Formation. The Xuanwei Formation can be subdivided into lower, middle, and upper members according to its lithology and coal-bearing properties. In terms of chronostratigraphy, the lower and middle members of Xuanwei Formation and the Emeishan Basalt Formation correspond to the Wuchiapingian, while the upper member of Xuanwei Formation corresponds to the Changhsingian (ICS (International Commission on Stratigraphy) 2018).

During the Late Permian, a wide range of palaeogeographical landscapes and hence environments of deposition were distributed in southwestern China (e.g., Shao et al. 1998). A belt of non-marine alluvial plain facies was developed in the eastern part of Yunnan, alongside the eastern margin of Kangdian Oldland. Marine-continental transitional and adjoining neritic facies belts were developed in most parts of western Guizhou (Fig. 1). The study

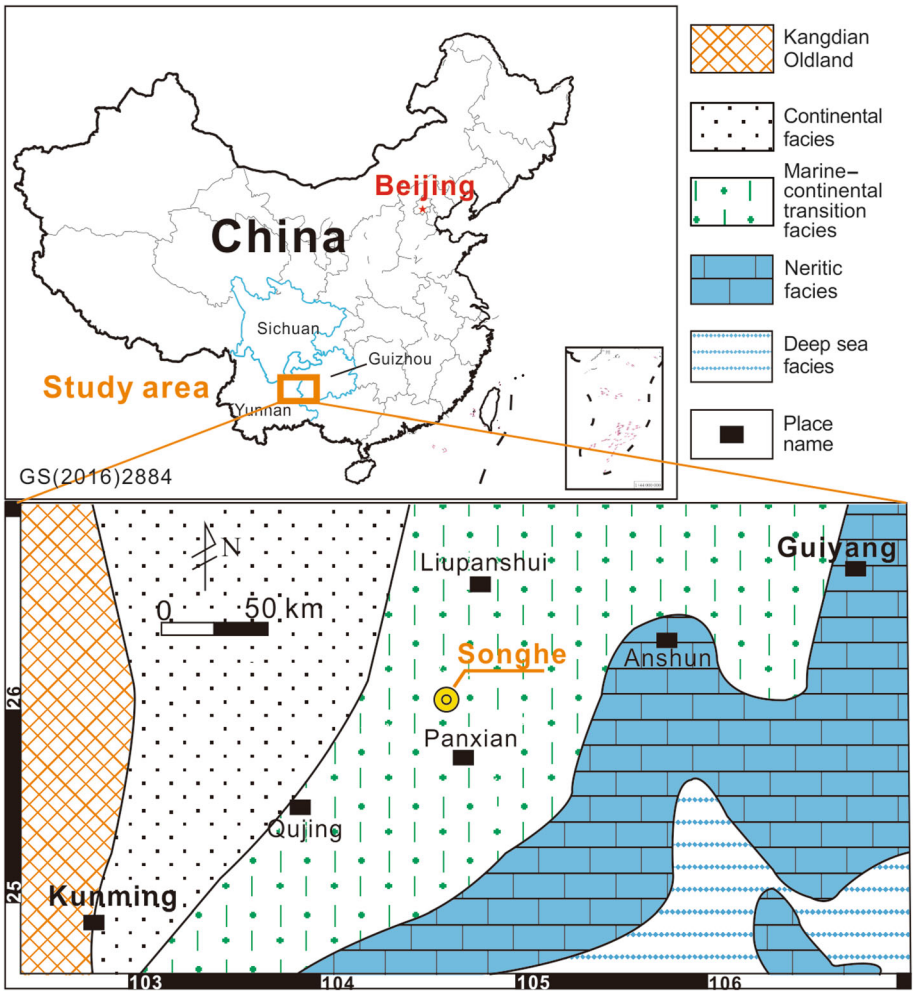

Fig. 1 Palaeogeography of eastern Yunnan and western Guizhou at the Late Permian (simplified from Shao et al. 1998) showing the position of the studied Songhe mining area. The map of China was modified after the National Bureau of Surveying and Mapping of China (No. GS(2016)2884)

area was situated in a paralic setting near the equator (Wang and Li 1998), where the peatlands were well developed during this period because of the prevalence of a warm and wet tropical climate (Tian and Zhang 1980; Guo 1990a).

3 Geophysical data and spectral analysis

The identification of orbital cycles within coal seams requires three inherent conditions: 1) no indication of a significant hiatus in the coal seam, 2) the depth series of the coal seams should span an orbital periodicity so that it can be treated as a time series (Schwarzacher 1993; Weedon 2003), and 3) no major tectonism occurred during the coal deposition. Three relatively thick and stable coal seams, 17# (5.6 m), 18# (6.4 m), and 17 + 18# (5.4 m), were investigated from three borehole sections in the Songhe mining area (Fig. 2). The lateral distances between each of two boreholes were less than 5 km.

These sections cover the stratigraphic intervals of the middle member of the Xuanwei Formation. Coal maceral analysis shows that: the 17# coal seam contains 86.9% vitrinite, 4.4% inertinite, 8.7% mineral matter, and minor liptinite; the 18# coal seam contains 75.9% vitrinite, 14.3% inertinite, and 9.8% mineral matter as well as minor liptinite; however there is no maceral data available for 17 + 18# coal seam (referring to the geological survey report of the Guizhou Administration of Coal Geology). The main coal quality parameters of the coal seams are given in the Table 1.

Geophysical logs represent properties of strata (Yu and Li 2003). Three types of geophysical logs are presented in Fig. 2: apparent resistivity (DLW), gamma-gamma (DEN), and natural-gamma (GR) of each researched coal section were chosen to reflect the changes of the mineral matter (ash) content (Diessel 1992). The change in maceral composition in coal seams could have potentially contributed to variations in the

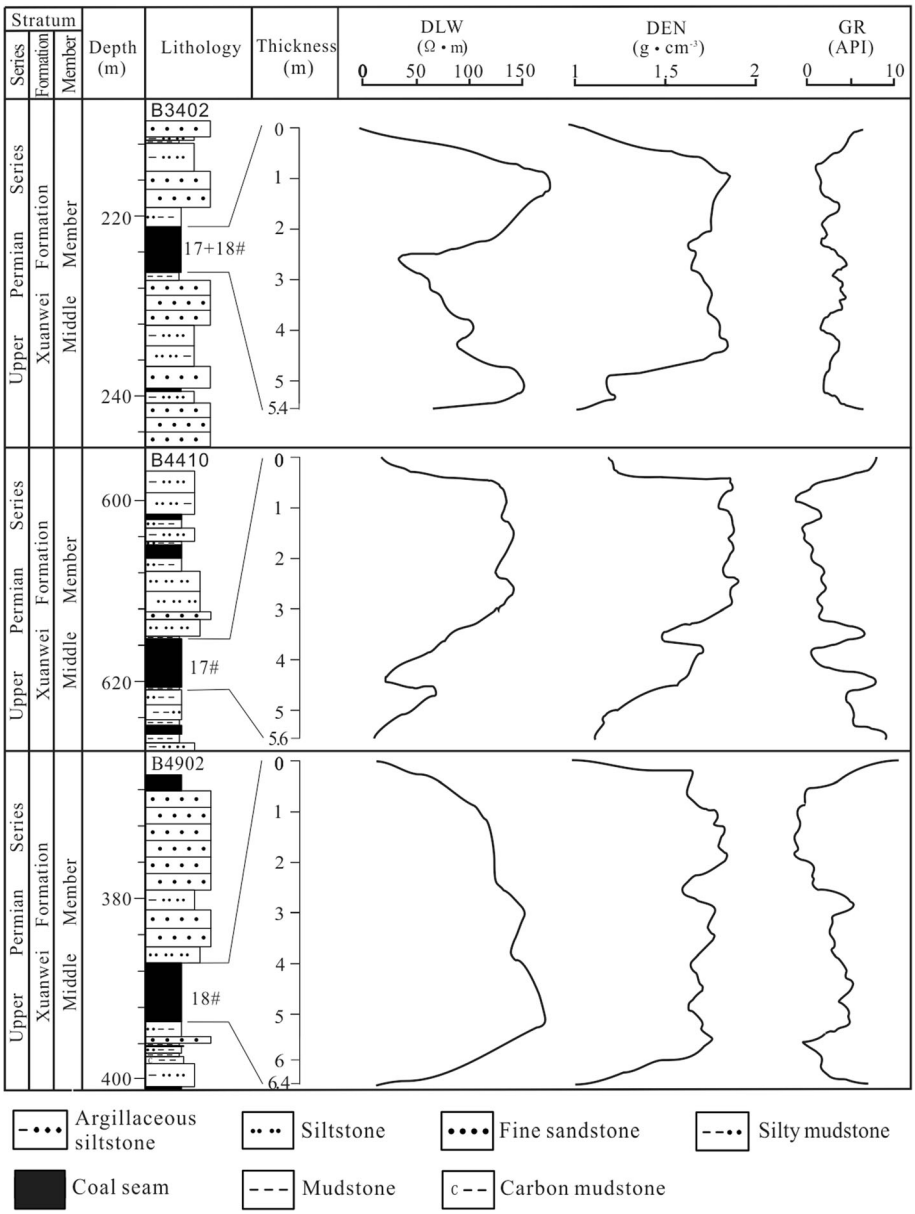

Fig. 2 Lithological and geophysical logs of the three Late Permian coal seams from the Songhe mining area, western Guizhou. DLW = Apparent resistivity; DEN = Gamma-gamma (Density); GR = Natural-gamma

Table 1 Main bulk coal quality parameters of the Late Permian coal seams from the Songhe mining area, western Guizhou

Coal Seam No.	A_d (%)	V_{daf} (%)	$S_{t,d}$ (%)	C_{daf} (%)	ARD ($g \cdot cm^{-3}$)
17#	17.41	21.03	0.40	79.63	1.33
18#	17.70	20.77	0.67	80.32	1.34
17 + 18#	NO DATA				

All data are from the geological survey report of the Guizhou Administration of Coal Geology

A Ash, *V* Volatile, S_t Total sulfur, *C* Carbon, *ARD* Apparent density, *d* Dry basis, *daf* Dry ash-free basis

geophysical log signals (Wang 2006) and even to the derivation of orbital cycles (Large et al. 2003). However, maceral-related oscillations were not considered in this study because vitrinite dominates (> 75%) in all the investigated coal seams.

All log data of the 17#, 18#, and 17 + 18# coal seams were obtained from the geological survey report in Songhe mining area (Guizhou Administration of Coal Geology 2002). These were recorded at a sampling interval of 0.1 m as originally sampled, i.e. 56, 64, and 54 points were measured, respectively. Spectral analysis was then undertaken to determine whether significant periodic oscillations occur in the

geological log signals, and whether or not these oscillations can be attributed to orbital climate forcing. In this study, the spectral analysis process was conducted using the SSA-MTM toolkit including singular spectrum analysis (SSA), multitaper method (MTM), and maximum entropy method (MEM) (Ghil et al. 2002). The SSA method was used to identify and remove the underlying low-frequency components in the data and meanwhile provide a non-linear reconstruction of significant frequency components. The MTM method was used to identify and compare significant frequencies in the proposed orbital range. The purpose of MEM is to check spectrum peaks whose confidence levels are 99% or more. For more specific information on operational processing please refer to http://research.atmos.ucla.edu/tcd//ssa/.

4 Results

Three main groups of frequencies, the 0.03–0.43, 0.52–0.74, and 0.85–1.23 cycles·m^{-1} in ascending order (Fig. 3), were obtained via spectral analysis and the averages were 0.20, 0.63, and 1.09 cycles·m^{-1}, labeled as f3, f2, and f1, respectively. Then the cycle lengths could be estimated using formula (1) as follows:

$$T = 1/f \quad (1)$$

where, T is the cycle length (m) and f is the frequency corresponding to f3, f2, and f1.

The calculations results for T3, T2, and T1 corresponding to f3, f2, and f1 were 5.0 m, 1.56 m, and 0.92 m, respectively. Then the ratio for the cycle length was 5.43:1.69:1, respectively, which is similar to the ratio for Milankovitch periodicities during the Late Permian at 250 Ma BP of 123 kyr (eccentricity), 35.6 kyr (obliquity), and 21.2 kyr (precession) = 5.8:1.7:1 (Berger et al. 1989, 1992). Thus, it is reasonable to conclude that these frequencies in coal seams could represent orbital cycles, because the information related to the Milankovitch cycles has been identified. This conclusion implies that the development of the peatland was continuous and undisturbed over long periods, and was driven to a significant extent by the Milankovitch cycles.

5 Period of coal deposition and the internal time framework construction

Following the identification of Milankovitch cycles, the rates of coal deposition were calculated using the following formula (2) (Fig. 5):

$$V_{coal} = T/t \quad (2)$$

where, V_{coal} is the rate of coal deposition (m·kyr^{-1}) expressed as the thickness of coal (m) deposited per thousand year (kyr^{-1}). T is the cycle length (m) of T1 (0.92 m), T2 (1.56 m), and T3 (5.0 m) as previously described in formula (1). t is the orbital periodicity (kyr) cited from Berger et al. (1992), with t1, t2, and t3 being 123 kyr (eccentricity), 35.6 kyr (obliquity), and 21.2 kyr (precession), respectively.

The V_{coal} values calculated based on the formula (2) range from 0.04 to 0.047 m·kyr^{-1}. Furthermore, the period of coal deposition can be estimated according to the formula (3) as follows:

$$T_{coal} = L/Vcoal \quad (3)$$

where, T_{coal} is the period of coal deposition (kyr). L is the thickness of coal (m) and V_{coal} is the rate of coal deposition (m·kyr^{-1}) obtained from formula (2).

As a result, the thickness of coal (L) of 5.6 m (17#), 6.4 m (18#), and 5.4 m (17 + 18#), in combination with the V_{coal} values calculated from formula (2), give rise to the estimated periods of coal deposition (T_{coal}) for the three seams. These are approximately: 140.8–119.8 kyr (17#), 160–136.2 kyr (18#), and 135–114.9 kyr (17 + 18#), respectively.

The periods of coal deposition calculated here are theoretically reasonable considering that the whole Wuchiapingian spans approximately 6.6 Ma (ICS (International Commission on Stratigraphy) 2018), which could provide a reasonable and, in our view, trustworthy recognition of the Milankovitch periodicities from geophysical logs in coal.

Following the calculation of the period of coal deposition, it is possible to subdivide this period into short and precise periods for the internal temporal framework of coal deposition on the basis of the wave curve corresponding to the specific frequency. The wave curve can be obtained by filtering of the respective log signals. Each one of two adjacent peaks or troughs constitutes one complete cycle, i.e., a complete orbital periodicity. Complete cycles could work as time measurement scales being used to subdivide the whole period of coal deposition into several relatively short and precise periods corresponding to different specific cycle lengths, i.e., specific orbital periodicities. In this study, the original geophysical log signals (DLW, DEN and GR) of each coal seam was filtered by the wavelet transformation method to obtain wave curves corresponding to the frequencies of f3 (0.20 cycles·m^{-1}), f2 (0.63 cycles·m^{-1}), and f1 (1.09 cycles·m^{-1}).

Eventually, three curves filtered from the DEN log signal of the 18# coal seam can appropriately subdivide the period of 18# coal seam deposition into relatively short and precise periods (Fig. 4), while other curves filtered from the investigated logs are less appropriate in this process. The 6.4-m thick coal seam (18#) was subdivided into one complete eccentricity periodicity of L2 (123

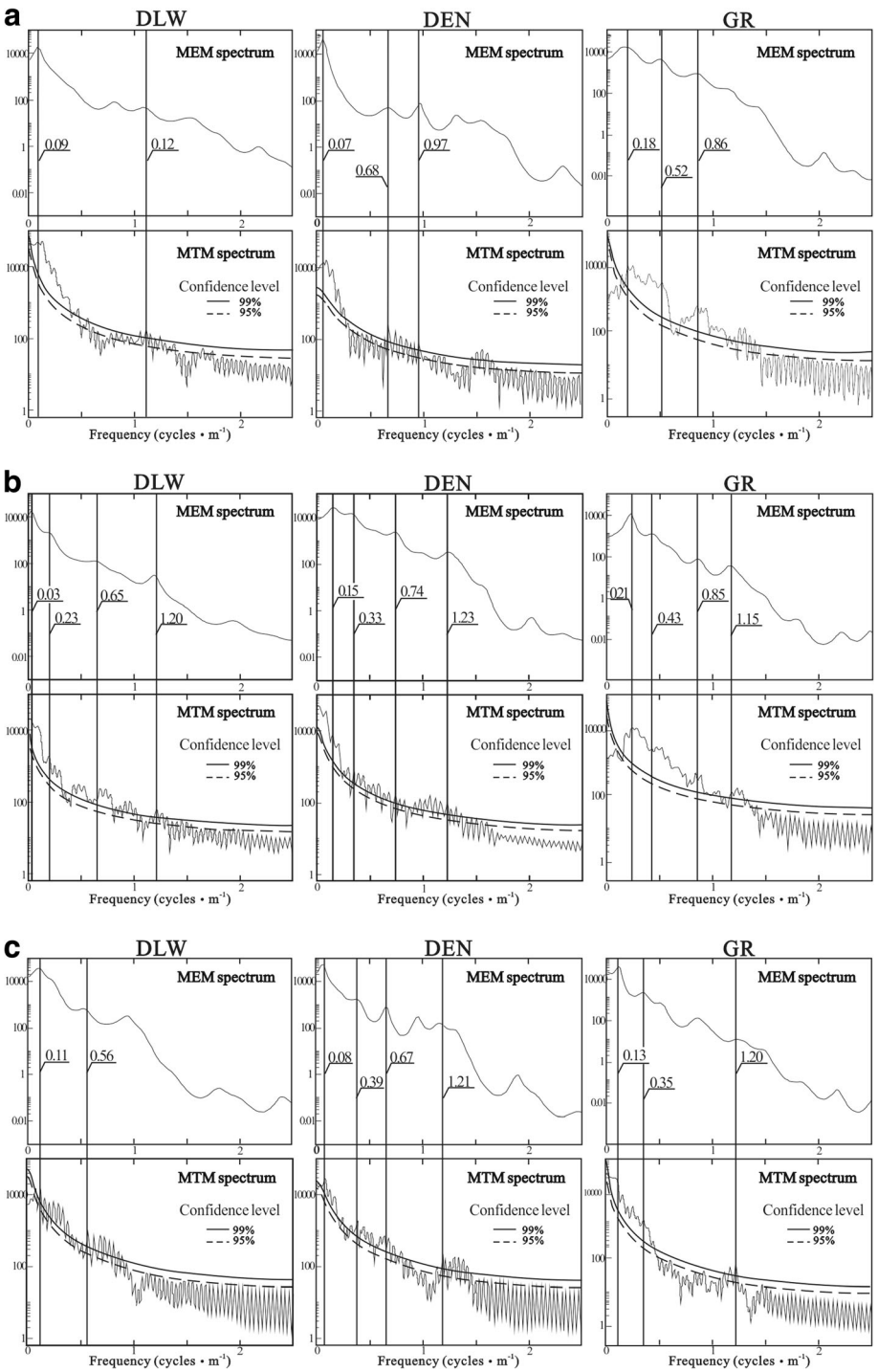

Fig. 3 Spectral analysis of the Late Permian coal seams from the Songhe mining area, western Guizhou. a, b, c show spectral analysis results of the 17 + 18#, 17# and 18# coal seams respectively. DLW, DEN (Density) and GR represent apparent resistivity, gamma-gamma and natural-gamma logs respectively. MEM and MTM represent the maximum entropy method and multitaper method respectively

kyr), three complete obliquity periodicities of M2 (35.6 kyr), M3 (35.6 kyr) and M4 (35.6 kyr), and five precession periodicities of S2 (21.2 kyr), S3 (21.2 kyr), S4 (21.2 kyr), S5 (21.2 kyr) and S6 (21.2 kyr) (Fig. 4). Different thicknesses of the subdivided coal seams equivalent to the same period of deposition indicate different rates of coal deposition: a thicker section implies a higher rate, while the thinner one represents a lower rate.

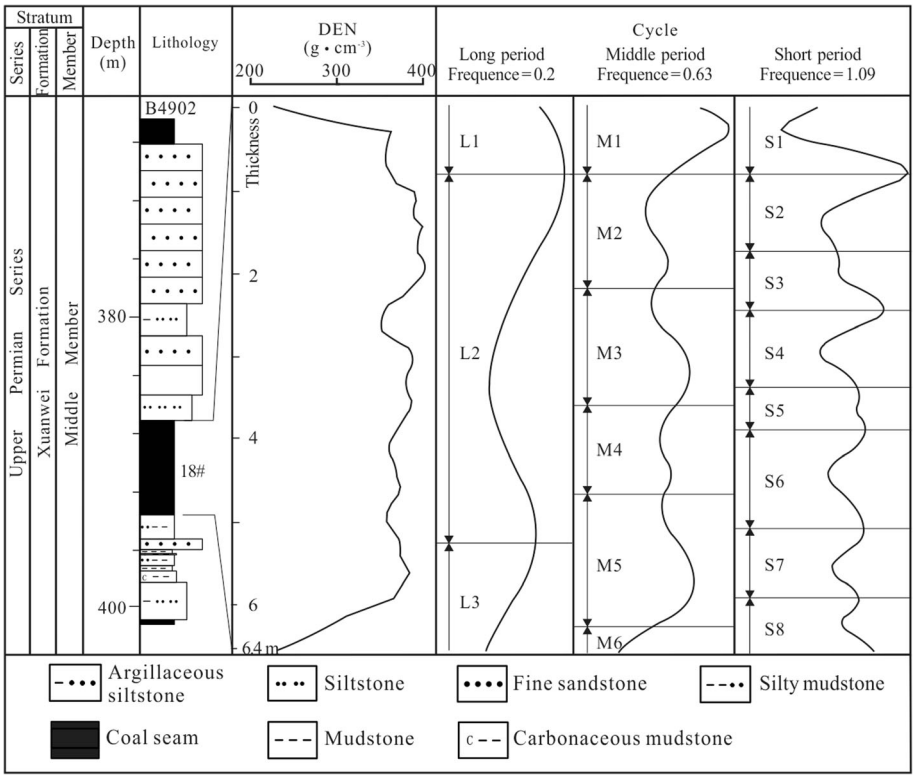

Fig. 4 The precise period division of the 18# coal seam by wavelet analysis. L, M and S represent Milankovitch periodicities of 123 kyr (eccentricity), 35.6 kyr (obliquity), and 21.2 kyr (precession), respectively

As for the reason of the insufficiently accurate subdivision of periods for the coal seams 17# and 17 + 18#, we think it is possibly because the incorrect choice of frequencies or other factors which may need more investigations.

6 Peatland productivity

For the calculation of peatland productivity, the long-term average carbon accumulation rate of the coal was calculated based on the following formula (4) (Fig. 5):

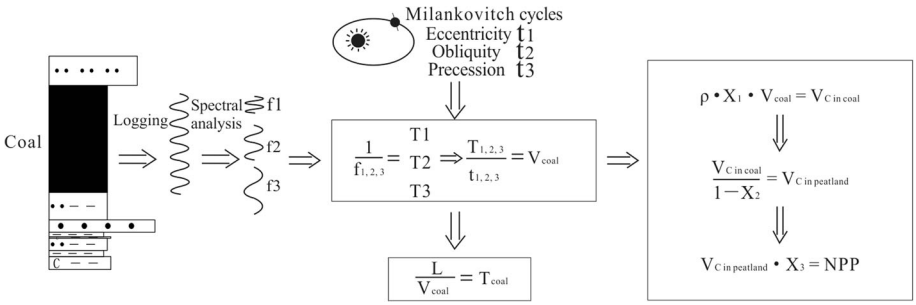

Fig. 5 Sketch showing procedures of the peatland productivity analysis. f1, f2, f3 represent the main average frequencies (cycles·m^{-1}) of the spectral analysis. t1, t2, t3 represent Milankovitch periodicities of 123 kyr (eccentricity), 35.6 kyr (obliquity), and 21.2 kyr (precession). T1, T2, T3 represent different cycle length (m). V_{coal} represents rate of coal deposition (m·kyr^{-1}). L represents thickness of coal seam (m). T_{coal} represents period of coal deposition (kyr). ρ is the measured dry bulk density of coal (g·cm^{-3}). X_1 is the measured average carbon concentration of the coal. X_2 is carbon loss percentage during the coalification. $V_{C\ in\ coal}$ represents the long-term average carbon accumulation rate for the coal (g·C·m^{-2}·a^{-1}). $V_{C\ in\ peatland}$ represents the long-term average carbon accumulation rate for the initial peatland (g·C·m^{-2}·a^{-1}). X_3 is the quantitative relation between the Holocene net primary productivity (NPP) level (g·C·m^{-2}·a^{-1}) and the long-term average carbon accumulation rate for the peatland

$$V_{C\ in\ coal} = \rho \times X_1 \times Vcoal \quad (4)$$

where, $V_{C\ in\ coal}$ is the long-term average carbon accumulation rate for the coal ($g{\cdot}C{\cdot}m^{-2}{\cdot}a^{-1}$) expressed as the amount of carbon (g) accumulated in an area (m^{-2}) per year (a^{-1}). ρ is the measured average density of the coal ($g{\cdot}cm^{-3}$). X_1 is the measured carbon concentration of the coal (%), and V_{coal} is the rate of coal deposition ($m{\cdot}kyr^{-1}$), which was described previously.

In this study, the measured average bulk densities of the 17# and 18# coal seams are 1.33 $g{\cdot}cm^{-3}$ and 1.34 $g{\cdot}cm^{-3}$ (Table 1). The measured average carbon concentrations are 79.63% and 80.32% respectively, which give similar estimates of the $V_{C\ in\ coal}$ values for the 17# and 18# coal seams of ca. 42.4–49.8 $g{\cdot}C{\cdot}m^{-2}{\cdot}a^{-1}$ and 43.0–50.6 $g{\cdot}C{\cdot}m^{-2}{\cdot}a^{-1}$, respectively. No geochemical data for the 17 + 18# coal seam is available, therefore we use the integrated data for the 17# and 18# coal seams (42.4–50.6 $g{\cdot}C{\cdot}m^{-2}{\cdot}a^{-1}$) as the representative value of the long-term average carbon accumulation rate for the coals investigated in this study.

Considering the carbon loss during coalification, the long-term estimated average carbon accumulation rate for the coal will be less than that in the initial peatland. According to the Van Krevelen diagram (Diessel 1992), it is suggested that when the carbon loses from the type III kerogen during the transition from peat to coal, hydrogen and oxygen will decrease simultaneously. Large and Marshall (2014) summarized the carbon loss during coalification of various maturity degrees of coal with different measured average carbon concentration and average dry bulk density. Based on this summary, the investigated coal seams with measured average carbon concentration of ca. 80% and average dry bulk density of 1.33 $g{\cdot}cm^{-3}$ lost ca. 30% carbon during coalification, i.e., ca. 70% carbon is retained in the coal. Thus, the long-term average carbon accumulation rate for the initial peatland can be calculated using the following formula (5) (Fig. 5):

$$V_{C\ in\ peatland} = V_{C\ in\ coal}/(1\text{-}X_2) \quad (5)$$

where, $V_{C\ in\ peatland}$ is the long-term average carbon accumulation rate for the peatland ($g{\cdot}C{\cdot}m^{-2}{\cdot}a^{-1}$) expressed as the amount of carbon (g) accumulated in an area (m^{-2}) of peat per year (a^{-1}). X_2 is the carbon loss percentage during the coalification, which is ca. 30% (Large and Marshall 2014). $V_{C\ in\ coal}$ is the long-term average carbon accumulation rate for the coal obtained from formula (4).

The $V_{C\ in\ peatland}$ value was determined to be ca. 60.6–72.3 $g{\cdot}C{\cdot}m^{-2}{\cdot}a^{-1}$, which is well within the range of long-term average carbon accumulation rates of the Holocene peatlands. The average carbon accumulation rates vary from 19.9 $g{\cdot}C{\cdot}m^{-2}{\cdot}a^{-1}$ in a boreal peatland (Korhola et al. 1995) to 100 $g{\cdot}C{\cdot}m^{-2}{\cdot}a^{-1}$ in a tropical peatland (Page et al. 2004; Lähteenoja et al. 2009) during the Holocene.

The temperature gradient and environmental conditions of the tropical area during the Late Permian were similar to those of current areas of peat deposition near the equator (Ziegler 1990; Ziegler et al. 1997). Based on this assumption, it is reasonable to evaluate the NPP of the Late Permian tropical peatland by applying the quantitative relation between the Holocene NPP level and the long-term average carbon accumulation rate for the peat expressed in the following formula (6):

$$NPP = V_{C\ in\ peatland} \cdot X3 \quad (6)$$

where, NPP is the net primary productivity of the peatland ($g{\cdot}C{\cdot}m^{-2}{\cdot}a^{-1}$). X_3 is the quantitative relation between the Holocene NPP level and the long-term average carbon accumulation rate for the peat in the tropic area. $V_{C\ in\ peatland}$ is the long-term average carbon accumulation rate for the peatland obtained from formula (5).

Such a comparison was made by Large (2007) and shows that the tropical NPP level was within the range of 300–900 $g{\cdot}C{\cdot}m^{-2}{\cdot}a^{-1}$ and the long-term average carbon accumulation rate for the peat varied from 50 to 250 $g{\cdot}C{\cdot}m^{-2}{\cdot}a^{-1}$ during the Holocene (Fig. 6). This indicates that the NPP level of peatland was approximately 4–6 times (X_3) of the long-term average carbon accumulation rate for the peatland in the tropics. Therefore, the NPP of tropical peatland during the Late Permian can be calculated as $Vc_{\ in\ peatland}$ (60.6–72.3 $g{\cdot}C{\cdot}m^{-2}{\cdot}a^{-1}$)·$X_3$ (4–6), which is 242–433.8 $g{\cdot}C{\cdot}m^{-2}{\cdot}a^{-1}$.

7 Discussion

The 17# and 18# coal seams with high ash content (Table 1) suggest the initial peatlands formed within a low-lying mire (Moore 1987) and were possibly rich in terrigenous siliciclasts deposited under an abundant surface water supply. Orbital variations could have affected climate change and further influenced precipitation and soil weathering, which are ultimately linked to the Milankovitch cycle forcing (Kerr 1981; Muller et al. 2008). Assuming that the local geological conditions were relatively stable during the period of peatland formation, the terrigenous debris content (such as ash) in coal from the water supply could serve as a medium for Milankovitch cycle research in some ways.

The conventional dating methods such as radiometric dating have already been widely used, however, it may be inadequate of providing sufficient accuracy required when constraining time for even relatively thick coal seams (Allègre 2008). The alternative method based on

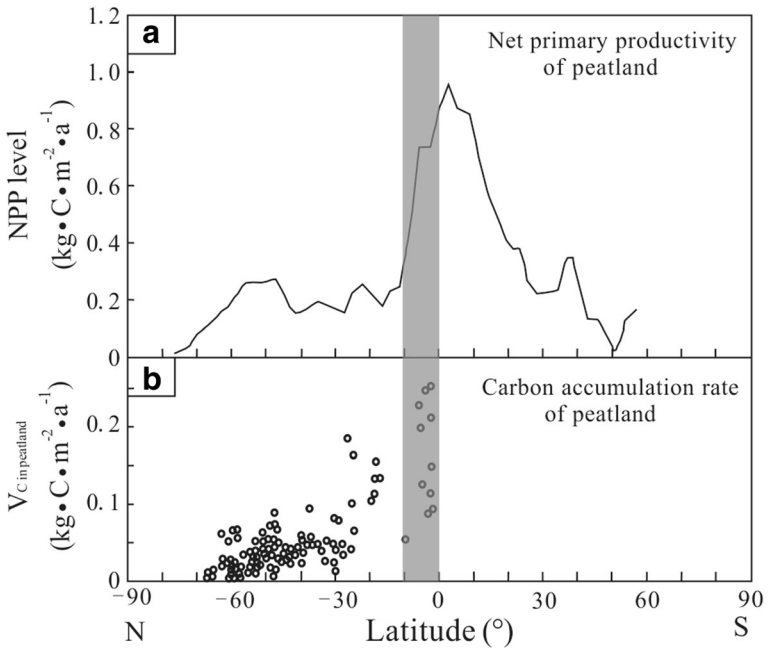

Fig. 6 Comparison of the latitudinal distribution of the Holocene NPP with the latitudinal variation in the carbon accumulation rate in peatland (modified after Large 2007). **a** The latitudinal distribution of the Holocene NPP; **b** The latitudinal variation in the carbon accumulation rate in peatland. The shaded area represents the latitude range of the study area during the Late Permian

Milankovitch cycles identified from geophysical data in coal to estimate the reasonable upper and lower limits of the coal deposition rate is more accurate (Large and Marshall 2014). For the Late Permian peatland, the estimated NPP levels are based on the available precise temporal framework of the coal seam.

The calculated Late Permian NPP values (242.4–433.82 $g{\cdot}C{\cdot}m^{-2}{\cdot}a^{-1}$) apparently correspond to the lower end of the range of the Holocene tropical peatland NPP (300–900 $g{\cdot}C{\cdot}m^{-2}{\cdot}a^{-1}$) (Fig. 6). The low rates of global terrestrial organic carbon burial, during the Lopingian could be due to aridity, global decrease in sea level, and transition from high biomass forests to low biomass herbaceous cover (Berner 2005; Hilton and Cleal 2007).

However, recent research suggests that the palaeoclimate was humid and warm during the Late Permian in southwestern China where tropical rainforests grew well and the coal-forming vegetation was relatively constant (Guo 1990b; Li et al. 1995). Some researchers have indicated that carbon production and storage of a peatland could have been subject to a palaeo-wildfire (Moore 1987); however, the inertinite content in the coal seams of this study area was less than 15%, indicating that the influence of palaeo-wildfire was small. The coal seams in the study area are relatively thick and stable, suggesting that the growth of the accommodation space was indeed consistent with the peat formation and the growth of the accommodation space was a favorable rather than a negative factor for NPP.

As mentioned above, temperature has a significant influence on photosynthesis efficiency. Modern research suggests that the study area was near the equator during the Late Permian, where the local mean annual temperature ranged from 26 °C to 29 °C without any significant difference from that of the present time (Fluteau et al. 2001). This suggests that temperature is not an important cause of the difference in local primary productivity at the study area.

Plants absorb CO_2 from the air and transform it into sugars and other carbon-based molecules during photosynthesis, and consume oxygen and break down organic matter during the respiration process. Given that the atmospheric composition has an influence on plant photosynthesis and respiration, the most likely factors for the productivity reduction are atmospheric O_2 and CO_2 concentrations. The models of Beerling and Berner (2000) and Berner et al. (2003) show that the global terrestrial biosphere NPP level will decrease by 11% with an increase of atmospheric O_2 concentration from 24% to 35%. The concentration of O_2 and CO_2 was 28% and 0.1% during the Late Permian respectively (shadowed column P_3–2 in Fig. 7), while it is 21% and 0.03% at the present time. Thus, it is reasonable to assume that relatively high CO_2 concentration level could have increased peatland productivity, while the high O_2 concentration level would counterbalance this effect, resulting in a lower NPP level. Similar conclusions were derived by Wang et al. (2011) from their research on Nuodong coal,

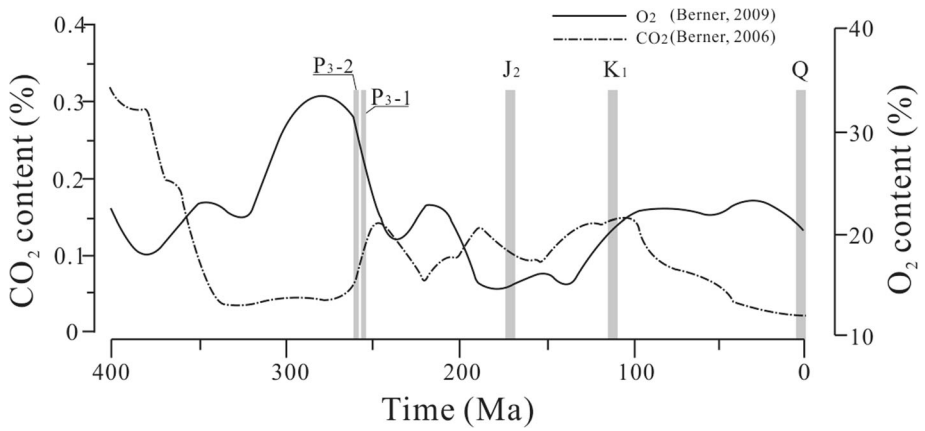

Fig. 7 Comparison of atmospheric CO_2 content (Berner 2006) and O_2 content (Berner 2009) through geological history. The shadow column P_3–2 represents the approximate time position of peatlands formed in western Guizhou during the Late Permian period in this study; P_3–1, J_2, K_1 and Q indicate the approximate time positions of peatlands formed in the Late Permian (Wang et al. 2011), the Middle Jurassic (Wang et al. 2018), the Early Cretaceous (Yan et al. 2016) and the Holocene (Large 2007), respectively

western Guizhou formed in the upper member of the Late Permian Longtan Formation, a period slightly younger than the coals in this study (shadowed column P_3–1 in Fig. 7). These conclusions were supported by more recent studies of the Middle Jurassic coals in the Ordos Basin (Wang et al. 2018) and the Early Cretaceous coals in the Erlian Basin (Yan et al. 2016) located in mid-latitude regions of the northern hemisphere.

To extend our understanding of the relationship between the atmospheric environmental conditions and the peatland NPP level, some findings of previous research on coals ranging in age from the Permian to the Quaternary are summarized below (Table 2). These enable comparison between tropical and mid-latitude long term average carbon accumulation rates of tropical and mid-latitude peat. Based on the linear equation for calculation of the Holocene long-term average rates of the carbon accumulation at different latitudes (Large and Marshall 2014) and the quantitative relation between the NPP level and the long-term carbon accumulation rates of the Holocene peatlands (Large 2007), we converted the Late Permian NPP level from the tropics to the mid-latitude region. The converted long-term average carbon accumulation rate of the peatland in the 40°–45°N regions is 28.7–40.4 $g \cdot C \cdot m^{-2} \cdot a^{-1}$ in this study and its corresponding NPP is 143.5–202 $g \cdot C \cdot m^{-2} \cdot a^{-1}$

Table 2 Summary of peatland net primary productivity (NPP) levels at different geological ages and latitudes

Geological age	Latitude	NPP ($g \cdot C \cdot m^{-2} \cdot a^{-1}$)	CO_2 content (%)	O_2 content (%)
P_3–1				
Late Permian	0°–(−10)°S	[b]217.2–462	0.1	28
P_3–2				
Late Permian	0°–(−10)°S	242–433.8	0.1	28
[a]P_3–1				
Late Permian	40°–45°N	112–243	0.1	28
[a]P_3–2				
Late Permian	40°–45°N	143.5–202	0.1	28
J_2				
Middle Jurassic	42°–44°N	256.7–307.1	0.1	14.6
K_1				
Early Cretaceous	40°–45°N	231–256	0.15	21
Q				
Holocene	40°–45°N	150–230	0.03	21

P_3–1, P_3–2, J_2, K_1 and Q refer to Fig. 7 for the approximate time positions of peatlands formed during geologic time
[a] means the converted value from the original tropics to a middle latitude area
[b] represents the new estimated NPP value based on the long-term average carbon accumulation rate for peatland (Wang et al. 2011)

($^{a}P_3$–2 in Table 2). Another Late Permian long-term average carbon accumulation rate for the peatland (Wang et al. 2011) was converted to a mid-latitude region of 22.4–48.6 $g{\cdot}C{\cdot}m^{-2}{\cdot}a^{-1}$ and its corresponding NPP level in tropical area was 112–243 $g{\cdot}C{\cdot}m^{-2}{\cdot}a^{-1}$ ($^{a}P_3$–1 in Table 2). Though this conversion may not be sufficiently rigorous and is largely based on the assumption of a degree of uniformitarianism, it can contribute to an understanding of the potential correlation between the NPP level and atmospheric environment expressed in the form of concentrations of O_2 and CO_2.

A comparison of the mid-latitude NPP levels between the Late Permian and the Middle Jurassic peatlands (Table 2; Fig. 7) demonstrates that the peatland NPP will increase when the atmospheric O_2 content markedly decreases while CO_2 content remains the same. Furthermore, a similar conclusion can also be drawn from the comparison of mid-latitudinal peatland NPP levels between the Late Permian and the Early Cretaceous with a remarkable decrease of O_2 content and a slight increase of CO_2 level. A comparison between the Early Cretaceous and modern peatland NPP levels illustrates that the peatland NPP levels will increase when the atmospheric CO_2 content increases and the O_2 content remains unchanged. Similarly, a comparison of mid-latitudinal peatland NPP levels between the Late Permian and the Holocene periods (Table 2; Fig. 7) show a decrease in peatland NPP level when CO_2 and O_2 contents simultaneously decrease, and even when the O_2 content changes more markedly.

Based on comparisons of peatland NPP levels among different geological ages and different latitudes, it is suggested that within the same latitudinal region the peatland NPP levels are largely influenced by temporal change in atmospheric CO_2 and O_2 contents. With a better understanding of the correlation between the peatland NPP and the atmospheric environment, coals can be used as a significant proxy to extend our high-resolution documentation and understanding of pre-Quaternary peatland ecology.

8 Conclusions

A pattern of Milankovitch periodicities of 123 kyr (eccentricity), 35.6 kyr (obliquity), and 21.2 kyr (precession) was identified by applying spectral analysis (apparent resistivity, gamma-gamma, and natural-gamma) to the geophysical logs of the Late Permian coal sections from the Songhe mining area in western Guizhou. The depositional periods of 17# (5.6 m), 18# (6.4 m), and 17 + 18# (5.4 m) coal seams were calculated as 140.8–119.8 kyr, 160–136.2 kyr, and 135–114.9 kyr, respectively.

Using Milankovitch periodicity as a temporal indicator, the Late Permian long-term average carbon accumulation rate for coals was estimated to be 42.4–50.6 $g{\cdot}C{\cdot}m^{-2}{\cdot}a^{-1}$. These values correspond to the long-term average carbon accumulation rate for the initial peatland of 60.6–72.3 $g{\cdot}C{\cdot}m^{-2}{\cdot}a^{-1}$ and the peatland NPP of 242.4–433.8 $g{\cdot}C{\cdot}m^{-2}{\cdot}a^{-1}$. The whole depositional period of the 18# coal seam of 160–136.2 kyr was further subdivided into short and precise periods by the wavelet analysis method corresponding to the Milankovitch periodicities. It includes one complete eccentricity cycle (123 kyr), three complete obliquity cycles (35.6 kyr), and five complete precession cycles (21.2 kyr). Different thicknesses of the subdivided coal seams equivalent to the same deposition periods indicates different rates of coal deposition, i.e., thicker seams imply higher rates while the thinner seams represent lower rates.

The present results indicate that when conditions of high rain fall and high humidity prevail in the palaeo-peatland at a given latitude, the rates of net primary productivity (NPP) vary with changes in atmospheric concentration of CO_2 and O_2. This relationship may help broaden the interpretation of NPP records to encompass considerations of changes in the composition of the atmosphere, at the particular part of the Earth's history for which coal records exist.

Acknowledgements

This work is supported by the National Natural Science Foundation of China (Grant No. 41572090).

Authors' contributions

ZY collected geophysical data and carried out this study and drafted the manuscript. LS gave critical and constructive comments on this manuscript and then revised it. DL conceived of the study and gave critical and constructive comments on an earlier version of this manuscript. HW participated in the design and data analysis of this study. BS gave constructive comments and revised this manuscript. All authors read and approved the final manuscript.

Competing interests

The authors declare that they have no competing interests.

Publisher's Note

Author details

[1]College of Geoscience and Surveying Engineering, China University of Mining and Technology (Beijing), Beijing 100083, China. [2]Faculty of Engineering, University of Nottingham, Nottingham NG7 2RD, UK. [3]Department of Earth Sciences, Natural History Museum, London SW7 5BD, UK.

Received: 11 December 2017 Accepted: 6 August 2018
Published online: 08 January 2019

References

Allègre, C.J. 2008. *Isotope geology*. Cambridge: Cambridge University Press.

Beerling, D.J., and R.A. Berner. 2000. Impact of a Permo-carboniferous high O_2 event on the terrestrial carbon cycle. *Proceedings of the National Academy of Sciences of the United States of America* 97 (23): 12428–12432.

Berger, A., M.F. Loutre, and V. Dehant. 1989. Pre-quaternary Milankovitch frequencies. *Nature* 342 (6246): 133.

Berger, A., M.F. Loutre, and J. Laskar. 1992. Stability of the astronomical frequencies over the earth history for paleoclimate studies. *Science* 255 (5044): 560–566.

Berner, R.A. 2005. The carbon and sulfur cycles and atmospheric oxygen from middle Permian to middle Triassic. *Geochimica et Cosmochimica Acta* 69 (13): 3211–3217.

Berner, R.A. 2006. Geocarbsulf: A combined model for Phanerozoic atmospheric O_2 and CO_2. *Geochimica et Cosmochimica Acta* 70 (23): 5653–5664.

Berner, R.A. 2009. Phanerozoic atmospheric oxygen: New results using the geocarbsulf model. *American Journal of Science* 309 (7): 603–606.

Berner, R.A., D.J. Beerling, R. Dudley, J.M. Robinson, and R.A. Wildman. 2003. Phanerozoic atmospheric oxygen. *Annual Review of Earth and Planetary Sciences* 31 (1): 105–134.

Briggs, J., D.J. Large, C. Snape, T. Drage, D. Whittles, M. Cooper, J.H.S. Macquaker, and B.F. Spiro. 2007. Influence of climate and hydrology on carbon in an Early Miocene peatland. *Earth and Planetary Science Letters* 253 (3–4): 445–454.

Diessel, C.F.K. 1992. *Coal-bearing depositional system*. New York: Springer-Verlag.

Fluteau, F., J. Besse, J. Broutin, and M. Berthelin. 2001. Extension of Cathaysian flora during the Permian: Climatic and palaeogeographic constraints. *Earth and Planetary Science Letters* 193 (3–4): 603–616.

Ghil, M., M.R. Allen, M.D. Dettinger, K. Ide, D. Kondrashov, M.E. Mann, A.W. Robertson, A. Saunders, Y. Tian, F. Varadi, and P. Yiou. 2002. Advanced spectral methods for climatic time series. *Reviews of Geophysics* 40 (1): 1–41.

Guizhou Administration of Coal Geology 2002. Geological Survey Report of Xinhua Coal Mine in Songhe mining area, Panxian County, Guizhou (in Chinese).

Guo, Y. 1990a. The palaeoclimate of late Permian in western Guizhou. *Coal Geology of China* 2 (3): 18–20 (in Chinese with English abstract).

Guo, Y. 1990b. Palaeoecology of flora from coal measures of upper Permian in western Guizhou. *Journal of China Coal Society* 15 (1): 48–49 (in Chinese with English abstract).

Han, D., and Q. Yang. 1980. *Coal geology of China (volume 2)*. Beijing: Publishing House of China Coal Industry (in Chinese).

Hilton, J., and C.J. Cleal. 2007. The relationship between Euramerican and Cathaysian tropical floras in the late Palaeozoic: Palaeobiogeographical and palaeogeographical implications. *Earth Science Reviews* 85 (3–4): 85–116.

ICS (International Commission on Stratigraphy), 2018. International Chronostratigraphic Chart. http://www.stratigraphy.org/ICSchart/ChronostratChart2018-08.pdf.

Kerr, R.A. 1981. Milankovitch climate cycles: Old and unsteady. *Science* 213 (4512): 1095–1096.

Korhola, A., K. Tolonen, J. Turunen, and H. Jungner. 1995. Estimating long-term carbon accumulation rates in boreal peatlands by radiocarbon dating. *Radiocarbon* 37 (2): 575–584.

Kremenetski, K.V., A.A. Velichko, O.K. Borisova, G.M. Macdonald, L.C. Smith, K.E. Frey, and L.A. Orlova. 2003. Peatlands of the western Siberian lowlands: Current knowledge on zonation, carbon content and Late Quaternary history. *Quaternary Science Reviews* 22 (5–7): 703–723.

Lähteenoja, O., K. Ruokolainen, L. Schulman, and M. Oinonen. 2009. Amazonian peatlands: An ignored C sink and potential source. *Global Change Biology* 15 (9): 2311–2320.

Large, D.J. 2007. A 1.16 ma record of carbon accumulation in Western European peatland during the Oligocene from the Ballymoney lignite, Northern Ireland. *Journal of the Geological Society* 164 (6): 1233–1240.

Large, D.J., T.F. Jones, C. Somerfield, M.C. Gorringe, B.F. Spiro, J.H.S. Macquaker, and B.P. Atkin. 2003. High-resolution terrestrial record of orbital climate forcing in coal. *Geology* 31 (4): 303–306.

Large, D.J., and C. Marshall. 2014. Use of carbon accumulation rates to estimate the duration of coal seams and the influence of atmospheric dust deposition on coal composition. *Geological Society, London, Special Publications* 404 (1): 1–9.

Li, X., G. Shen, and B. Tian. 1995. *China floras in geological history*. Guangzhou: Science and Technology of Guangzhou Press (in Chinese).

Li, X., and X. Wu. 1996. Late Paleozoic phytogeographic provinces in China and its adjacent regions. *Review of Palaeobotany and Palynology* 90 (1–2): 41–62.

Liu, B., X. Xu, X. Pan, H. Huang, and Q. Xu. 1993. *Sedimentary crust evolution and mineral formation of South China*. Beijing: Science Press (in Chinese).

Liu, G. 1990. Permo-carboniferous paleogeography and coal accumulation in North China and South China continental plates. *International Journal of Coal Geology* 16 (1): 73–117.

Mitsch, W.J., and J.G. Gosselink. 2007. *Wetlands (the fourth Edition)*. New York: Wiley.

Moore, P.D. 1987. Ecological and hydrological aspects of peat formation. *Geological Society, London, Special Publications* 32 (1): 7–15.

Muller, J., M. Kylander, A. Martinez-Cortizas, R.A.J. Wüst, D. Weiss, K. Blake, B. Coles, and R. Garcia-Sanchez. 2008. The use of principle component analyses in characterising trace and major elemental distribution in a 55 kyr peat deposit in tropical Australia: Implications to paleoclimate. *Geochimica et Cosmochimica Acta* 72 (2): 449–463.

Page, S.E., J.O. Rieley, and C.J. Banks. 2011. Global and regional importance of the tropical peatland carbon pool. *Global Change Biology* 17 (2): 798–818.

Page, S.E., R.A.J. Wűst, D. Weiss, J.O. Rieley, W. Shotyk, and S.H. Limin. 2004. A record of Late Pleistocene and Holocene carbon accumulation and climate change from an equatorial peat bog (Kalimantan, Indonesia): Implications for past, present and future carbon dynamics. *Journal of Quaternary Science* 19 (7): 625–635.

Schwarzacher, W. 1993. *Cyclostratigraphy and the Milankovitch theory*. Amsterdam: Elsevier.

Shao, L., H. Liu, B. Tian, and P. Zhang. 1998. Sedimentary evolution and its controls on coal accumulation for the late Permian in the upper Yangtze area. *Acta Sedimentologica Sinica* 16 (2): 55–60 (in Chinese with English abstract).

Tian, B., and L. Zhang. 1980. *Fossil atlas of Wangjiazhai mining area Shuicheng Guizhou*. Beijing: Coal Industry Press (in Chinese).

Vitt, D.H. 1994. An overview of factors that influence the development of Canadian peatlands. *Memoirs of the Entomological Society of Canada* 169: 7–20.

Wang, D., Z. Yan, H. Liu, D. Lü, and Y. Hou. 2018. The net primary productivity of mid-Jurassic peatland and its control factors: Evidenced by the Ordos Basin. *International Journal of Mining Science and Technology* 2: 177–185.

Wang, H., L. Shao, D.J. Large, and P.B. Wignall. 2011. Constraints on carbon accumulation rate and net primary production in the Lopingian (late Permian) tropical peatland in SW China. *Palaeogeography, Palaeoclimatology, Palaeoecology* 300 (1–4): 152–157.

Wang, J. 2006. *Practical manual for new methods and technology of modern coal exploration, coal mine geophysical exploration and logging*. Beijing: China Coal Industry Press (in Chinese).

Wang, J.D., and H.M. Li. 1998. Paleo-latitude variation of Guizhou terrain from Devonian to cretaceous. *Chinese Journal of Geochemistry* 17 (4): 356–361.

Wang, Y., and Y. Jin. 2000. Permian palaeogeographic evolution of the Jiangnan Basin, South China. *Palaeogeography, Palaeoclimatology, Palaeoecology* 160 (1): 35–44.

Weedon, G.P. 2003. *Time-series analysis and Cyclostratigraphy: Examining stratigraphic Records of Environmental Cycles*. New York: Cambridge University Press.

Yan, Z., L. Shao, S. Wang, D.J. Large, H. Wang, and Q. Sun. 2016. Net primary productivity and its control factors of early cretaceous peatlands: Evidence from no. 6 coal in the Jiergalangtu sag of the Erlian Basin. *Acta Sedimentologica Sinica* 34 (6): 1068–1076 (in Chinese with English abstract).

Yu, J., and Z. Li. 2003. Wavelet transform of logging data and its geological significance. *Journal of China University of Mining and Technology* 32 (3): 336–339.

Yu, Z. 2011. Holocene carbon flux histories of the world's peatlands: Global carbon-cycle implications. *Holocene* 21 (5): 761–774.

Yu, Z., J. Loisel, D.J. Charman, D.W. Beilman, and P. Camill. 2014. Holocene peatland carbon dynamics in the circum-arctic region: An introduction. *Holocene* 24 (9): 1021–1027.

Ziegler, A.M. 1990. Phytogeographic patterns and continental configurations during the Permian period. In *Geological society of London memoir 12: Palaeozoic Palaeogeography and biogeography*, ed. W.S. McKerrow and C.R. Scotese. London: Geological Society of London.

Ziegler, A.M., M.L. Hulver, and D.B. Rowley. 1997. Permian world topography and climate. In *Late glacial and postglacial environmental changes: Quaternary, carboniferous-Permian, and Proterozoic*, ed. I.P. Martini. New York: Oxford University Press.